Mechanisms of Fluid-Mud Interactions Under Waves

Robert A. Dalrymple, John H. Trowbridge, Dick K.P. Yue , Samuel J. Bentley, Gail C. Kineke,
Yuming Liu, Chiang C. Mei, Lian Shen, Peter A. Traykovski,
c/o Dept of Civil Engineering
The Johns Hopkins University
3400 North Charles Street
Baltimore, MD 21218
phone: (410) 516-7923 fax: (410) 516-7473 email: rad@jhu.edu

Award Number: N00014-06-1-0718
http://www.ce.jhu.edu/dalrymple/MURI

LONG-TERM GOALS

The goals of this project are to investigate the mechanisms for wave dissipation in the presence of bottom mud. These mechanisms are being examined via field measurements in the Gulf of Mexico, laboratory experiments of waves over a mud bottom, and numerical and theoretical analyses. Implementation of these various damping mechanisms into numerical models provides the ability to not only predict wave behavior over mud, but also to infer from the sea surface the nature of the bottom material.

OBJECTIVES

We are measuring wave damping due to mud off the coast of Louisiana, quantifying the dynamics of the bottom mechanisms responsible for the dissipation of wave energy. We are examining different mechanisms for the damping of wave energy by bottom mud in the laboratory and through the use of theoretical and numerical models. These damping mechanisms include the direct forcing of the mud by the wave-induced bottom pressure and velocities; indirect forcing through nonlinear surface wave effects (including wave groups); resonant forcing of interfacial waves at the water/mud interface; damping and shear instabilities in the lutocline; and large scale broadband mechanisms that involve a complex sea state and a combination of the above mechanisms.

APPROACH

The approach involves a field effort, involving experiments within a mud patch offshore the coast of Louisiana; a laboratory effort, examining the above mechanisms in a controlled environment; and a theoretical and numerical approach, with the ultimate objective of providing numerical models that include wave damping over mud.

The field work consisted of three field campaigns (a 2007 pilot study and field experiments in the spring of 2008 and 2010) of wave and bottom measurements. The experiments involved the use of bottom-mounted quadrapods that support acoustical instruments to measure the horizontal and vertical

Report Documentation Page

Form Approved
OMB No. 0704-0188

1. REPORT DATE	2. REPORT TYPE	3. DATES COVERED
30 SEP 2011		**00-00-2011 to 00-00-2011**

4. TITLE AND SUBTITLE	5a. CONTRACT NUMBER
Mechanisms of Fluid-Mud Interactions Under Waves	5b. GRANT NUMBER
	5c. PROGRAM ELEMENT NUMBER
6. AUTHOR(S)	5d. PROJECT NUMBER
	5e. TASK NUMBER
	5f. WORK UNIT NUMBER
7. PERFORMING ORGANIZATION NAME(S) AND ADDRESS(ES) **The Johns Hopkins University,Dept of Civil Engineering,3400 North Charles Street,Baltimore,MD,21218**	8. PERFORMING ORGANIZATION REPORT NUMBER
9. SPONSORING/MONITORING AGENCY NAME(S) AND ADDRESS(ES)	10. SPONSOR/MONITOR'S ACRONYM(S)
	11. SPONSOR/MONITOR'S REPORT NUMBER(S)

12. DISTRIBUTION/AVAILABILITY STATEMENT
Approved for public release; distribution unlimited

13. SUPPLEMENTARY NOTES

14. ABSTRACT

15. SUBJECT TERMS

16. SECURITY CLASSIFICATION OF:			17. LIMITATION OF ABSTRACT	18. NUMBER OF PAGES	19a. NAME OF RESPONSIBLE PERSON
a. REPORT	b. ABSTRACT	c. THIS PAGE			
unclassified	**unclassified**	**unclassified**	**Same as Report (SAR)**	**17**	

structure of the velocity and concentration and motion of the sediment at the bottom. In addition, a surface buoy provides atmospheric measurements. Two of the quadrapods are located at the seaward and landward ends of the experimental area to provide estimates of the directional wave spectrum and energy flux into and out of the study area In addition, cores of the seabed have been taken to determine recent depositional history, porosity, and mixing depth. Finally echo-sounding of the entire extent of the measurement profiles was conducted.

Laboratory experiments of waves over muds are being made in two experimental facilities. The first is a shaker table that supports a water/mud tank. This small-scale tank is oscillated to excite wave motion and then stopped so that the decay of the wave motion can be measured for a given mud layer. The second is an 18m long wave tank outfitted with a 10 m long, 10 cm deep mud patch within a false bottom. A string of acoustic and wire wave gages measure the decay of the waves down the tank.

The theory and numerical modeling effort consists of synergistic theoretical consideration, CFD analyses, and direct wavefield simulations (DWS). Regular and multiple scales perturbation analyses with the incorporation of realistic frequency dependent mud rheology have been developed to understand the basic characteristics and damping mechanisms for nearshore wave propagation for relatively simplified wave/mud conditions. CFD analyses based on fully nonlinear Navier-Stokes equation incorporating different mud rheology models are used to investigate the effects of shear instability and turbulence in water and mud layer and to develop equivalent bottom friction coefficient for wave prediction. DWS are developed, based on the integration of the theoretical studies, CFD developments, tank measurements, and field experiments conducted in this project, for the prediction of wavefield evolution over a muddy bottom and topography.

WORK COMPLETED

Three field experiments have been completed and data are being analyzed. Both shipboard measurements (bottom samples, soundings, and multi-beam sonar) and instrumented bottom array experiments have been carried out. In the laboratory, two experimental series were done in both the wave tank and a shaker table apparatus. The shaker table experiments are completed. The wave tank tests have shown the development of an instability of the mud/water interface. This instability only appears when the lutocline is within centimeters of the free surface. Wave damping over the mud has been examined for both an incident wave train as well as wave groups. The theory and modeling effort focused on the study and comparison of the effects of different mud rheology on the wave attenuation and on the assessment of the effects of different interaction mechanisms in different conditions by utilizing theoretical methods, CFD analyses, and advanced direct wave simulation (DWS). Specifically, we incorporated existing mud models for perturbation analyses and direct simulations. We performed analytical studies of attenuation of nonlinear long and short waves over Newtonian viscous mud and visco-elastic mud. We conducted CFD analyses of high amplitude waves over thin visco-elastic mud. We developed and integrated modeling of broadband wave attenuation into DWS, compared DWS results with field measurements, and investigated the effect of nonlinear two-layer resonances (water-mud layers) in wave attenuation.

RESULTS

Shipboard Measurements--One of the underlying hypotheses for our study is that the potential for wave attenuation is greatest when and where the largest volume of fluid mud is present. Previous studies and our work have shown that high concentration mud suspensions are delivered alongshore seasonally from the Atchafalaya River, ~100 km east of the study area. Once delivered to the study area, these suspensions are subject to local reworking by waves and onshore/offshore transport by waves, currents, and gravity. Our three years of field study incorporates evaluation of both spatial and temporal variability at scales of meters to kilometers, and days to years, during years with distinctly different river-supply terms, as shown by annual hydrographs of the Atchafalaya River (Fig. 1). We have measured activities and calculated sediment inventories of the cosmogenic radioisotope ^{7}Be (half life 53.3 days); the highest inventories are indicative of sediment recently derived from a major fluvial source, which is the Atchafalaya River in our case. By documenting changing inventories of ^{7}Be in the seabed, we can follow the movement across space and time of sediment freshly deposited from a fluvial source. The short half life allows rapid radioactive decay, according to $I_t=I_0\exp(-\lambda t)$, where I_0 is initial inventory of ^{7}Be, t is time, and $\lambda=0.013$ day^{-1}, the ^{7}Be decay constant. Over the course of 30 days, the typical sampling interval for our field study, the inventory of ^{7}Be in one location will decrease by 33%, unless new sediment is deposited locally (increasing the inventory) or sediment is eroded (decreasing the inventory) (Fig. 2). X-radiography of sediment cores in which ^{7}Be is measured also provides a record of distinct events that influence ^{7}Be inventories, in the form of freshly deposited beds, and erosive contacts that indicate removal of sediment.

Figure 2 illustrates averaged decay-corrected change in ^{7}Be inventory from one sampling period to the next, for all three field seasons (2007, 2008, 2010). In 2007, a persistent increase in ^{7}Be inventory from February to April indicates the transport of fresh sediment from the Atchafalaya, probably from the flood pulse shown just prior to February 2007 sampling in Figure 1. Conversely, 2008 trends suggest that modest input in Feburary-March was followed by no net input in March-April, consistent with the peak in river discharge that occurred after April 2008 sampling.

The magnitude of ^{7}Be inventory change both temporally (Fig. 2) and spatially (Fig. 3) is indicative of significant local sediment transport that is probably associated with fluid mud formation. For example, the net mass transport between sampling events can be estimated from the change in inventory, specific ^{7}Be activity of the sediment, and sediment porosity. For typical surface sediment porosities of ~0.9 and specific ^{7}Be activities of 1-3 dpm/g (disintegrations per minute/gram), a decay-corrected inventory increase of 1 dpm/cm^2 (February-March in 2007 and 2008, Fig. 2) suggests net sediment deposition of 0.4-2.5 g for the period between measurements, or a layer 1.6-10 cm thick at a porosity of 0.9. These estimates are consistent with surficial bed thicknesses evident in X-radiographs that are indicative of sediment transport events days to weeks before sampling occurred.

In 2008, time-series measurements with high concentration Optical Backscatterance Sensors mounted at 20 cmab (OBS5 Campbell Scientific) at the all three tripod sites indicated periods during wave events of $\geq$50 g/l suspended-sediment concentrations. These concentrations yield a mass of sediment of 1 g/cm^2 or greater within a nearbed high-concentration layer, of the same order as the estimate of sediment deposition from ^{7}Be measurements. All sites sampled for bottom sediment between 3 and 10 m water depth, over all sampling periods, showed surface bulk densities of <1.3 g/cm^3 (a reasonable threshold for fluid mud) for ~ 50% of the samples at each site. The presence of these low bulk densities

(though variable in space and time), high concentration resuspension events, and changes in ^{7}Be indicate a dynamic seabed with common, though episodic, presence of fluid mud coinciding with period of high sediment discharge and cold front activity. These high-concentration suspensions impact wave attenuation and ultimately the along- and across-shore sediment dispersal.

Observation and modeling of laminar-turbulent transitions in fluid mud flows studied by Traykovski and Hsu contributed to new of concepts developed by Bentley relating hydrodynamics of fluid muds to fabric of sedimentary event beds within fluid-mud deposits (Macquaker, Bentley, and Bohacs, 2010). Sedimentary fabric observed in X-radiographs for this study, and in a previous STRATAFORM study (Bentley and Nittrouer, 2003) suggests that the transition from turbulent to laminar flow conditions within some fluid-mud flows produces a diagnostic microstratigraphy that is preserved in both modern and ancient deposits, and can be used as a paleo-indicator for these flow conditions (Macquaker, Bentley, and Bohacs, 2010).

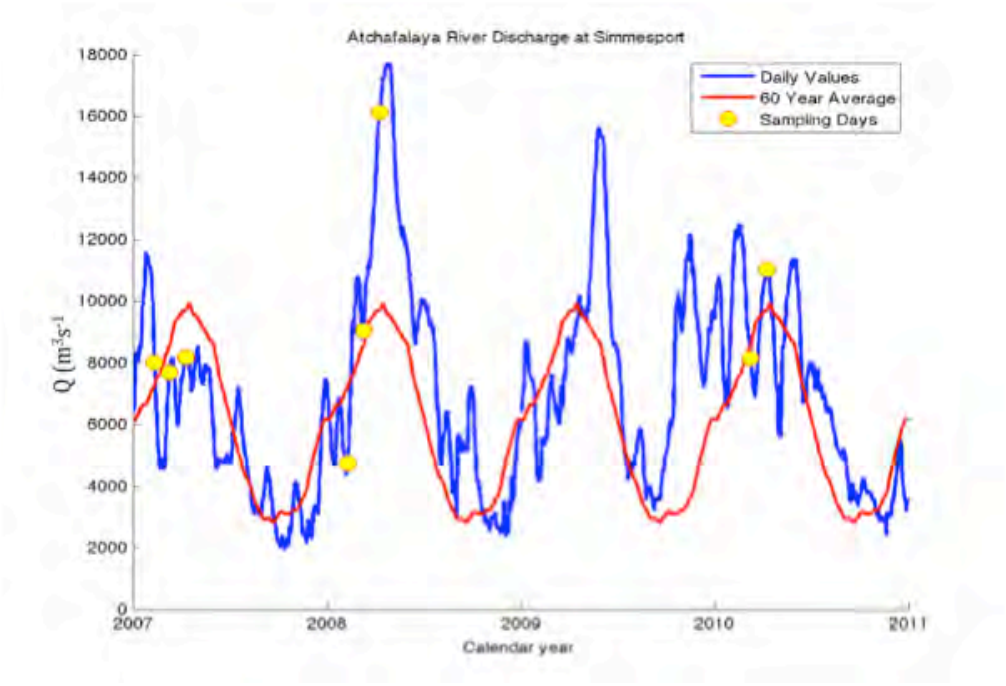

Figure 1. Daily and mean discharge for Atchafalaya River, showing sampling dates for 2007, 2008, and 2010. The Atchafalaya River is the primary source of fine mud delivered to our study area.

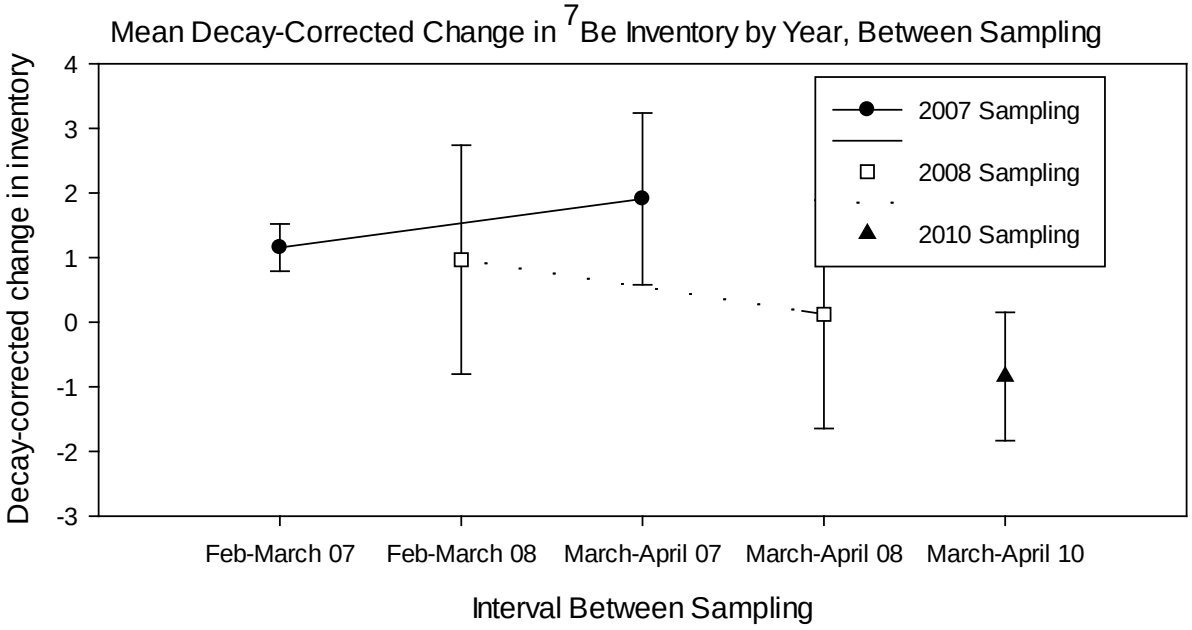

Figure 2. Decay-corrected change in ^{7}Be inventories averaged for each sampling period. Increase or decrease of mean inventory suggests either delivery or removal of sediment recently derived from the Atchafalaya fluvial source. Error bars indicate 1 standard deviation of mean.

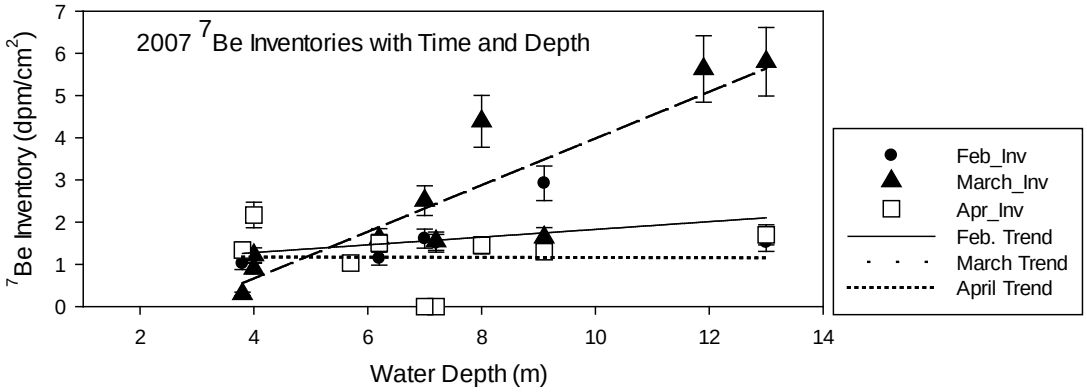

(a)

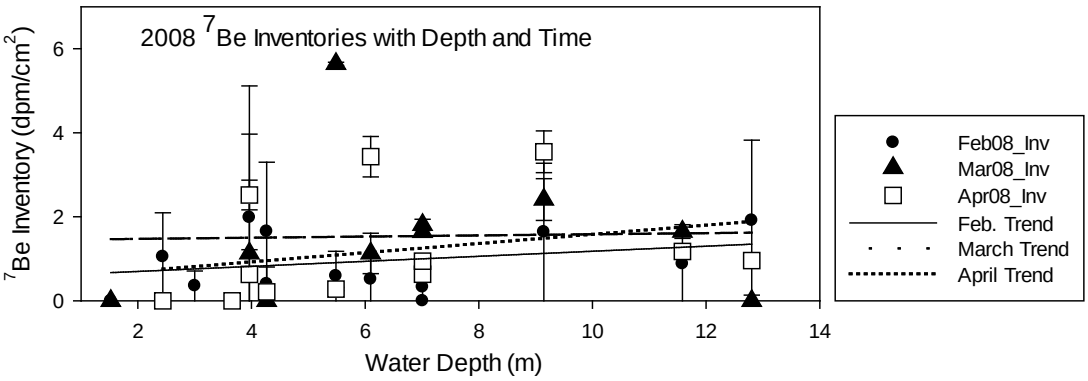

(b)

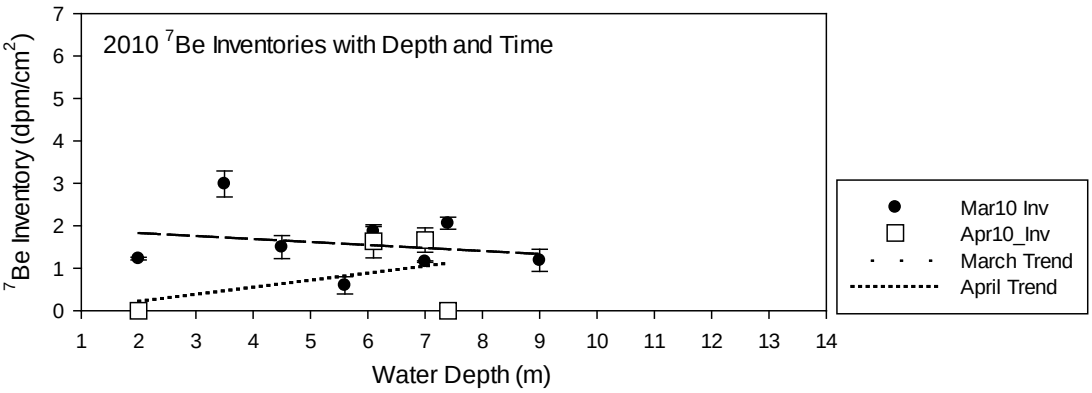

(c)

Figure 3. Inventories of ^{7}Be for all cores in each field season, showing linear regression of inventory versus depth for each sampling period. Error bars indicate the integrated analytical error for each core. (A)2007 cores; (B) 2008 cores; (C) 2010 cores.

In-situ measurements of mud layer boundary processes and wave energy loss: In 2011 we are continuing to analyze the data collected in the 2008 and 2010 field programs. In 2008 instruments were deployed on the 5, 7 and 9 m isobaths to measure wave energy flux divergence and bottom boundary layer process responsible for the wave attenuation. In 2010 the instruments were deployed in shallower water depths of 3, 5 and 7 m as attenuation rates are typically higher in shallow water. In 2008 the outer sites contained upward looking Nortek AWAC (acoustic wave and current) profiler to measure waves and the central site contained single frequency pulse coherent Doppler profiler (PC-DP) capable of measuring wave boundary layer and turbulence resolving velocity profiles through the mud layer. In 2010, we upgraded the single frequency PC-DP to multiple frequency processing to improve the range velocity ambiguity associated with single frequency processing (Traykovski and Jaffre, 2011).

The analysis of both data sets revealed a consistent picture whereby wave energy flux divergence dF/dx, is greatest during storms since there is the most energy available to dissipate and then decreases as wave heights decrease as the storm wanes (Figure 4b). However, the normalized attenuation rate $k = dF/dx/F$ was typically low (~ 0.1 km^{-1}) during storms, but increased by a factor of 2 to 4 as the storm waned and the fluid mud layers began to consolidate while remaining mobile (Figure 1a and c). The 2010 data revealed that there can be considerable spatial variability to these processes, and that the paradigm suggested by Elgar & Raubenheimer (2008) of greatest k in shallow waters based on data averaged over several storms, is not necessarily true on short time scales. Our 2010 dF/dx and k measurements revealed that attenuation often decreased in 3 to 5 m depths during storms and increased offshore in 5 to 7 m water depths. One contributing factor to this could be the presence of wave supported gravity flows in the mud layer (Figure 4e), (Traykovski, 2007).

Both the 2008 and 2010 data sets suggest the dominant mechanism for the transition from high dF/dx, low k during storms to low dF/dx, high k after storms is a consequence of a turbulent to laminar flow transition within the mud layer. This can be seen in the estimates of turbulent dissipation rate (e_t) form the 2008 data (Figure 1f), which decreases dramatically as the flow in the mud layer laminarizes and k increases. Figure 5 shows PC-DP acoustic intensity, horizontal and vertical velocity profiles over a few waves for both laminar and turbulent flow from the 2010 data set. The acoustic intensity reveals small fluctuation on the lutocline during laminar flow and large fluctuations during turbulent flow. The upper region of the mud layer moves with approximately equal horizontal velocity to the water layer. The vertical velocity images and spectra reveal the water layer is turbulent with a $f^{-5/3}$ spectral decay above the wave peak at 0.15 Hz. In the turbulent case the mud layer shows a similar spectra, while in the laminar flow case turbulent fluctuations fall off more steeply than $f^{-5/3}$ until reaching the sensor noise floor of P_{ww} ~ 5e-7 $(m/s)^2/Hz$ at f > 1.5 Hz. During these periods of laminar flow k is maximized and given knowledge of the mud layer thickness can be predicted by viscous dissipation models such as Dalrymple & Liu (1977).

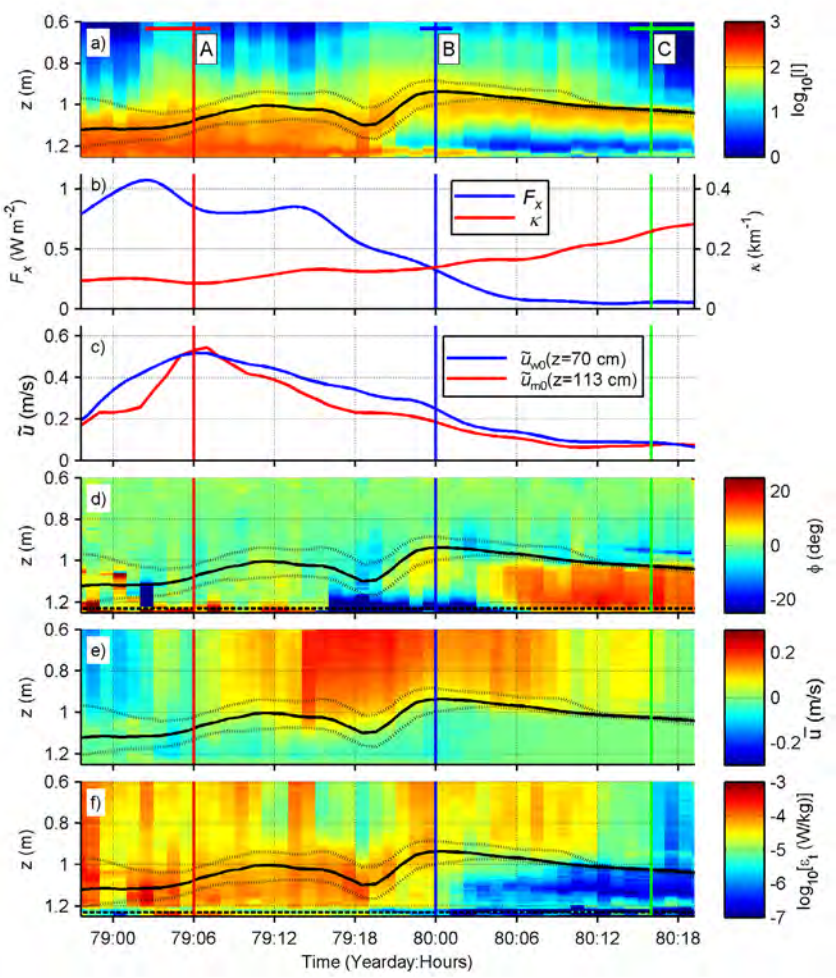

Figure 4. Time series of boundary layer measurement from the PCDP. a) PCDP backscattered intensity with colored vertical lines in the turbulent (red), transitional (blue), and laminar (green). The solid black line indicates the burst median location of the lutocline and the dashed lines indicate the location of the crests and troughs of the internal mode fluctuations. The increase of acoustic attenuation produces a backscatter minima within the mud layer as consolidation begins b) F_x and κ. c) Wave orbital velocity amplitudes above ($\tilde{u}_{0w}$) and below ($\tilde{u}_{0m}$) the mud water interface. d) Phase (ϕ) of wave boundary layer velocity relative to freestream. A consistent phase lead of 15 to 20 is observed during the high κ laminar flow period. e) Mean across-shore currents ($\overline{u}_{0w}$) showing an offshore gravity flow in the mud layer from 79:06 to 80:03 (light blue region) . f) Inertial dissipation method estimates of Turbulent dissipation (ε_i)

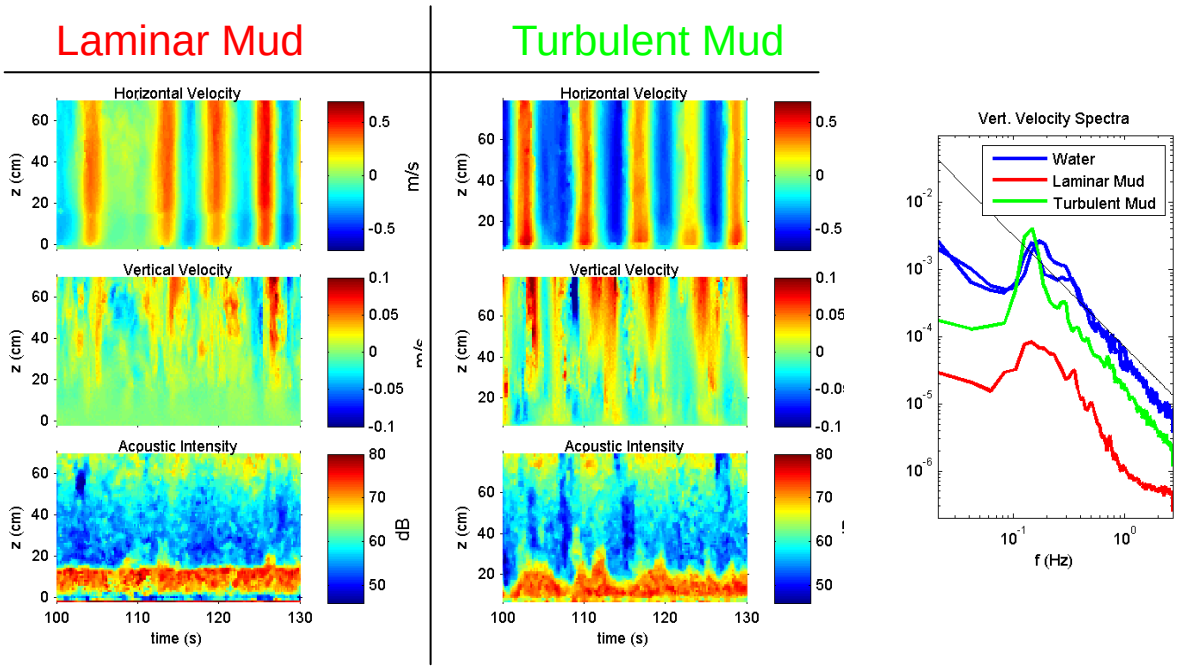

Figure 5. PC-DP acoustic intensity, horizontal and vertical velocity profiles and over a few waves for both laminar and turbulent flow from the 2010 data set. Spectra of vertical velocity in both the mud layers show reduced high frequency fluctuations during periods of laminar flow in the mud layer, while flow remain turbulent in the water layer

Laboratory experiments—The laboratory work has consisted of two separate sets of tests: the shaker table, which examines the decay of standing waves over mud, and the wave tank, where experiments on wave damping are carried out, using progressive waves of different frequency and amplitude with different mud thicknesses.

One of the interesting phenomena observed in other investigator's work has been the increase or decrease of wave damping with wave steepness. For example, Yamamoto and Schuckman (1984) show an increase with steepness and Tsuruya and Nakano (1987) and Maa (1986) show a decrease. In our shaker table experiments, testing shortly after stirring up the bottom mud into the water column, the wave damping does not change with wave steepness, while, when testing with mud that has settled for two days and its behavior is more like a mud rather than a fluid mud, the damping increases with steepness. The history of the mud (the amount of settling time, the amount of working by waves) plays an important role.

Last year, we reported on an instability of the lutocline that occurred when the lutocline was within a few centimeters of the water surface. This three-wave instability led to generation of subharmonic standing waves in the lutocline. Further testing showed that the superharmonic waves are generated as well and a further instability leads to patches of coherent turbulent structures within the standing waves. This is depicted in Figure 6.

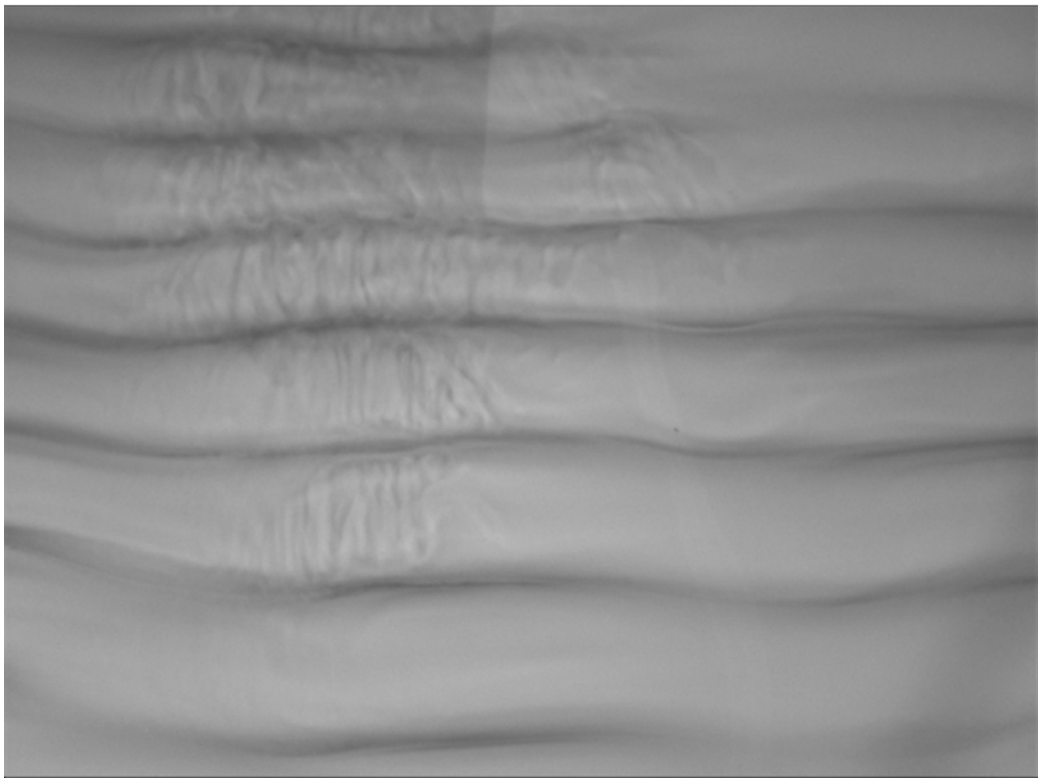

Figure 6. Subharmonic standing waves on the surface of the lutocline, generated by a long surface wave train traveling from left to right in the figure. Superharmonic waves (hard to see) and the turbulent structures (middle left) within the subharmonic waves are also present.

Theoretical modeling—We have extended the recent work by Mei, Krotov, Huang and Huhe (2010, JFM) to study long waves over a sloping beach. The main objective is to examine the effects of the realistic rheology on the wave motion and the feedback effect on mud. Since the Stokes expansion used by Mei et al. for intermediate wavelength fails in very shallow water, a theory similar to the Boussinesq approximation is used instead.

The theory is developed under the following assumptions: inviscid fluid over a thin layer of viscoelastic fluid-mud, and the ratios of water depth to wave length, wave amplitude to water depth and mud thickness to water depth are all comparably small as the bed slope. An asymptotic theory is developed for the evolution and attenuation of periodic waves and of the mud-water interface. Higher harmonics generated in the surface waves by nonlinearity is damped by to the dissipation in the mud layer. Numerical results have been worked out to show the effects of different rheology as well as wave steepness, mud depth and bed slope, etc. Data of mud samples from two field sites are taken because they have very different rheological features. In particular, fluid-mud from Hangzhou Bay, China (Huhe and Huang, 1994) is weakly elastic and almost Newtonian. On the other hand, mud from Gulf of Mexico, analyzed by Prof R. A. Dalrymple and K. Melick, is highly elastic. Using the measured data at four frequencies within the range of $0.1 < \omega < 10$ rad/s, we have determined the constitutive coefficients of a generalized viscoelastic law between stress and strain, shown in figure 7. The evolution of waves over a sloping layer of fluid-mud have been computed from the asymptotic

equations for the following simple bathymetry: shallow sea of constant depth in $-\infty < x < 0$ connected to a plane beach of constant slope in $0 < x < x_s$. Numerical solutions have been obtained for the first ten surface-wave harmonics A_m, m = 1, 2, · · · , 10. The initial conditions are prescribed at the offshore edge of the beach so that $A_1(0) = 1$, $A_m(0) = 0$, m = 2, 3, 4, ...,10. Rheological data for mud samples from Hangzhou Bay and Gulf of Mexico are taken from figure 1.

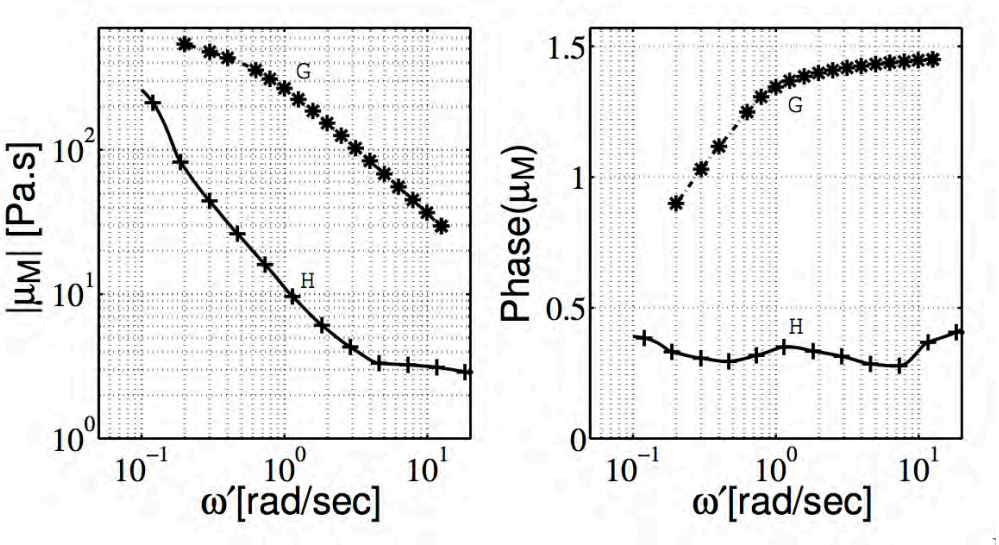

Figure 7: Phase and modulus of the complex viscosity of fluid mud from Hangzhou Bay (H) and Gulf of Mexico (G).

We cite only one example with the following inputs: d = 0.3 *m*, ω = 0.25 *rad/s* (wave period T = 15.7s), and h_0 = 3 *m*. Thus the incident wavenumber is $k = \omega/\sqrt{gh_0} = 0.0461\ m^{-1}$. The dimensionless parameters are δ = 0.1 (ratio of mud thickness to maximum water depth) and κ = 0.1383 (maximum water depth to wavelength/2π). The incident wave amplitude is chosen to be A = 30 *cm* corresponding to ε = A/h = 0.15. The dimensionless bed slope is s = 1/5, corresponding to the physical slope of S = sκ = 0.02766. The first three harmonics of the surface and the interface are shown in figures 8 and 9. Of the two samples, the Gulf of Mexico mud has the greater viscosity and rigidity; the dominant harmonic $|A_1|$ is understandably smaller over most of the slope. Spatial undulations due to nonlinear energy exchanges among harmonics are greatly suppressed. All the interface harmonics B_m are much smaller, implying weak motion in the mud layer, which must be caused by the much larger elasticity (or rigidity). In contrast, exchanges between harmonics due to nonlinearity are much more prominent in the less viscous and more Newtonian Hangzhou Bay mud. Note the spatial modulation in of harmonics over the Hangzhou Bay due to greater nonlinearity. Note also that surface wave amplitude vanishes on the shoreline, quite unlike waves on a beach with a rigid bottom.

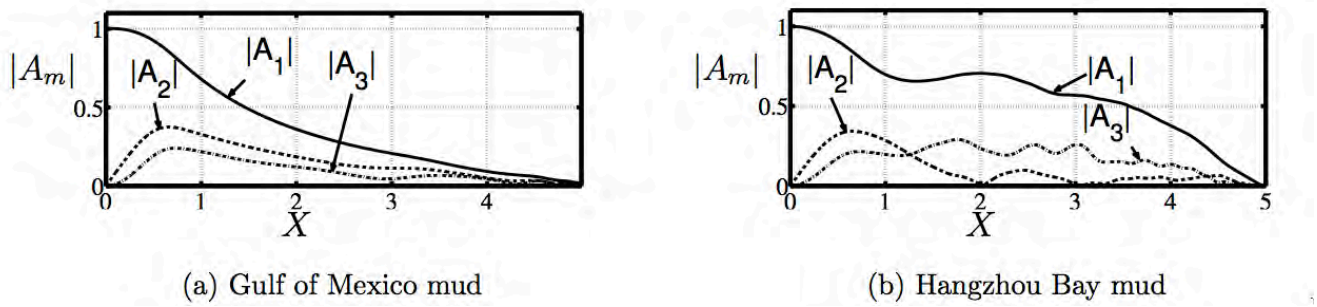

Figure 8 Evolution of the first three harmonics of the free surface over different muddy seabeads. For ε=0.15 and s= 1/5, δ=0.1

In a Newtonian viscous fluid, it is well known that there is a steady drift (Eulerian streaming) in the oscillatory boundary layer near the solid wall due to nonlinear convective inertia. In the viscoelastic fluid-mud the corresponding response is a static elastic deformation that is manifested in the change of mud thickness. Computations are in progress. A paper will be completed shortly for publication.

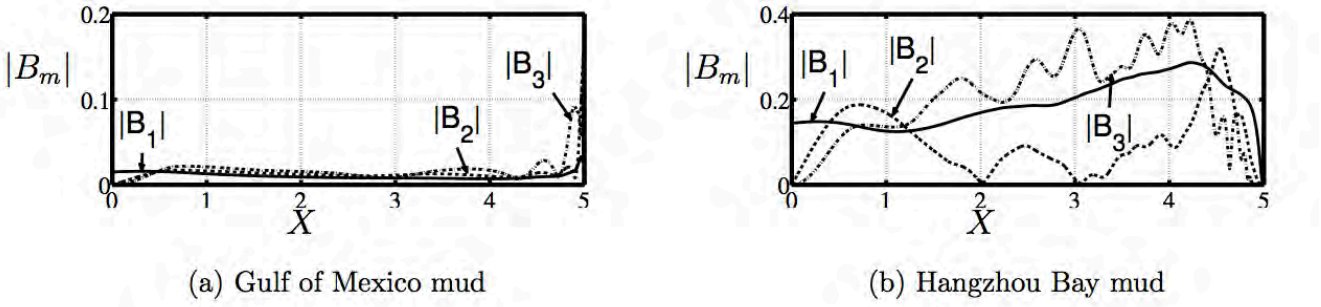

Figure 9 Evolution of the first three harmonics of the interface for different muddy seabeds. The vertical scales are different for two muds. For ε = 0.15, s = 1/5, δ = 0.1.

Finally Professor Z.H. Huang of Singapore has provided us with the rheological data of mud from Hanzhou Bay, China. He is also contributing to the theoretical tasks.

Numerical modeling--We are investigating theoretically and computationally the indirect mechanism for dissipation of short surface waves through their near-resonant interactions with long sub-harmonic waves that are dissipated by the bottom. Using direct perturbation analysis and energy argument, we obtained analytic predictions of the evolution of the amplitudes of two short primary waves and the long sub-harmonic wave, elucidating the energy transfer from the short waves to the long wave, which may be significant over time. We obtained expressions for the rate of total energy loss of the system, showing that this rate has an extremum corresponding to a specific value of the (bottom) damping coefficient (for a given pair of short wavelengths relative to water depth). These analytic results agree

very well with direct numerical simulations developed for the general nonlinear wave-wave and wave-bottom interaction problem. Despite the canonical problem we consider involving a single triad, the results provide a physically plausible explanation of recent observations of strong short wave attenuation as they travel over (dissipative) muddy sea floors (Sheremet & Stone 2003; Sheremet et al. 2005; Elgar & Raubenheimer 2008).

Figure 10a shows the time evolution of the amplitudes of the two primary short waves (a_1 and a_2) and the sub-harmonic (long) wave (a_-), which form a near-resonance triad. Both the theoretical prediction and direct simulation result are shown. The results are obtained with the short wave frequencies $\omega_1(g/h)^{1/2} = 0.48$ and $\omega_2(g/h)^{1/2} = 0.65$ and the bottom dissipation coefficient of sub-harmonic wave $\beta_- / \omega_- = 0.60$, where $\omega_- = \omega_2 - \omega_1$ and h is water depth. The evolution is marked by near monotonic decrease in amplitude of the shorter a_2 wave, (partially) compensated by the monotonic increase of amplitude a_1 of the longer primary wave. The evolution of the sub-harmonic wave (a_-) takes the form of a damped oscillation settling after some time towards a steady-state finite asymptotic value. The rate of decrease of a_2 is always greater than the rate of increase of a_1, leading to the decrease of the total energy of the system in time. The comparisons between the theory and direct numerical simulation are remarkably satisfactory. Figure 10b plots the total dissipation rate of the system (via damping of the long sub-harmonic wave) as a function of the dissipation coefficient (β_-) of the sub-harmonic wave with $\omega_1(g/h)^{1/2} = 0.48$ and $\omega_2(g/h)^{1/2} = 0.65$. The analytical solution is compared with the direct simulation result. The agreement between them is reasonably good. Both the analytical solution and direct simulation result show that there is an extremum in the dissipation of the system achieved at a particular value of β_-. The derivation of the theory and detailed comparisons with direct simulations are presented in Alam, Liu & Yue (2011).

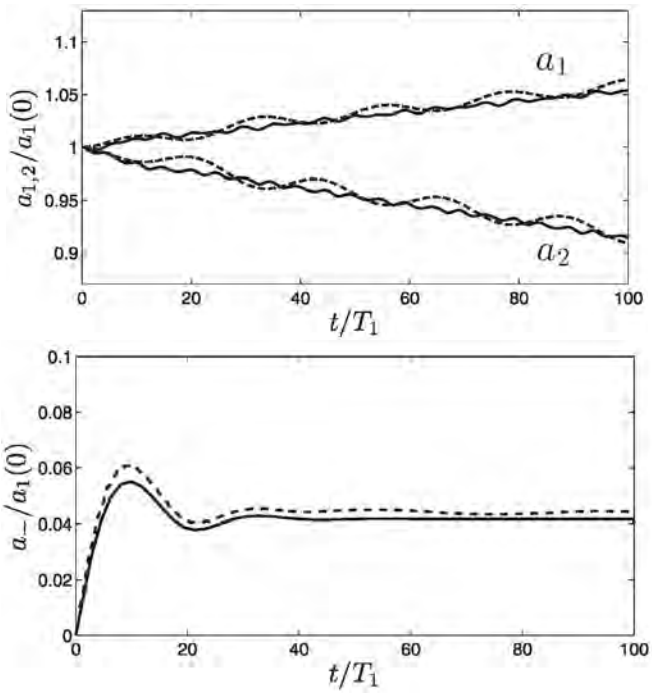

(a)

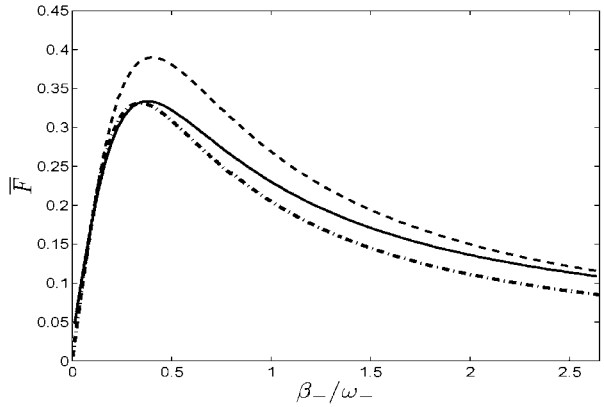

(b)

Figure 10. (a) Time evolution of the amplitudes of primary short waves (a_1 and a_2) and sub-harmonic long wave (a_-) obtained by theory (- - -) and direct numerical simulation (—). (b) Dimensionless damping rate of the (near-resonance triad) wave system as a function of damping coefficient β_- of the sub-harmonic wave: direct simulation result (—) and theoretical solutions from perturbation theory (- - -) and energy argument (- · - · -).

Additionally, a highly accurate, direct numerical simulation model has been developed for water waves propagating over fluid mud. The model uses the level-set method to capture the dynamic evolution of the surface wave and the mud-water interfacial wave. From simulations, substantial details of the

water and mud flow fields and new insights to the energy transport and dissipation processes in the coupled flow system are obtained. Both non-breaking and breaking waves are investigated.

In the study of non-breaking wave, the surface wave and the water-mud interfacial wave have finite amplitude. The simulation data provide a detailed description of velocity and vorticity fields in the water and mud. The nonlinear wave effect is quantified, and the wave energy dissipation rate is compared with theoretical predictions. The energy transfer mechanism at the water-mud interface is analyzed in detail. In addition, the processes of energy transport and dissipation in the water-mud system are elucidated.

For the first time, a plunging breaker over fluid mud is simulated to investigate the effect of muddy seabed on wave breaking. It is found that in the presence of mud, the intensity of wave breaking is reduced compared with no-mud case, the dissipation in water reduces, and the dissipation in mud plays an important role in wave energy evolution. Before the impingement of plunging jet on the wave surface and then after about 2.5 wave periods when most of the wave energy is lost, dissipation in mud dominates that in water. During the wave breaking itself, the dissipation rate in water increases sharply and exceeds that in mud. The above process is shown in the representative result plotted in Figure 11.

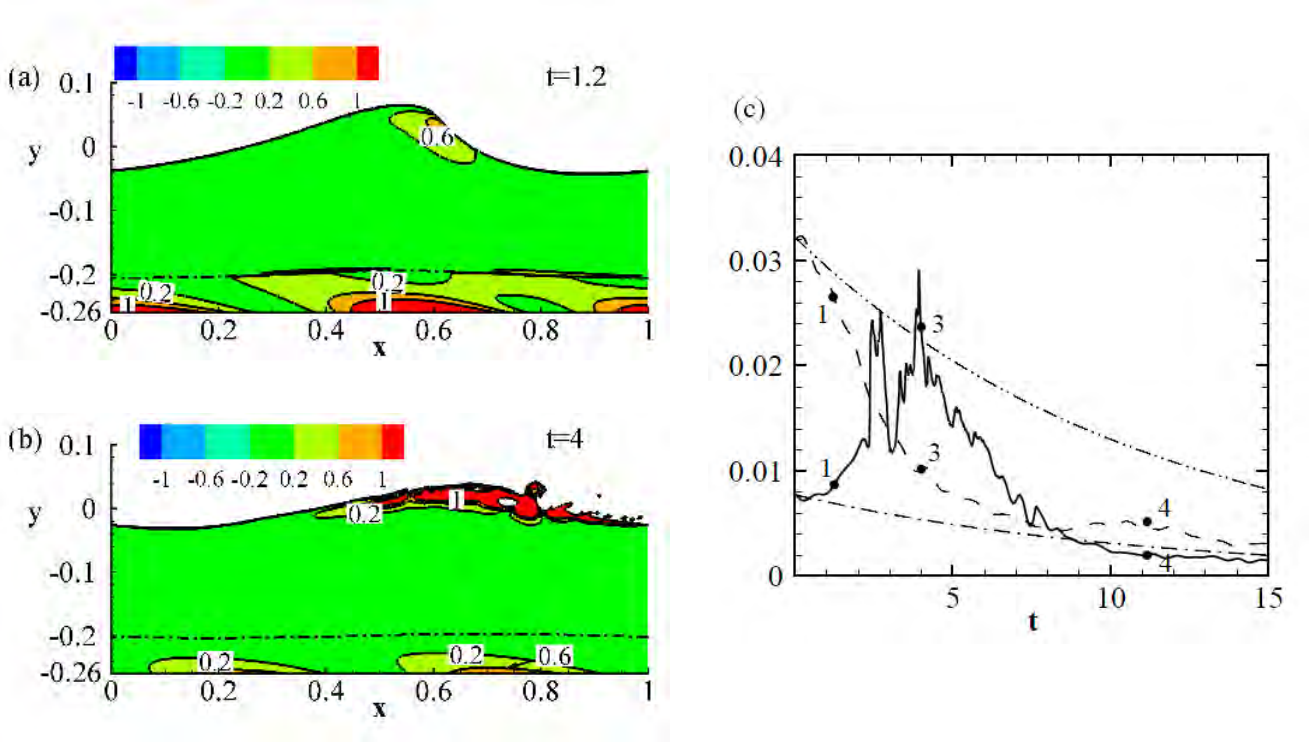

Figure 11. Viscous dissipation rate in wave breaking over mud simulated by CFD. Plotted on the left are the contours of viscous dissipation rate (a) before and (b) during the breaking. The water-mud interface is marked by – □ –. The dissipation rate is normalized by $E_w(0)\sigma$. Here $E_w(0)$ is the initial water wave energy and σ is the wave angular frequency. Plotted on the right, in (c), is the time history of total normalized viscous dissipation rate in the water (----) and mud (- - -). The dissipation rates of a non-breaking case are also plotted for comparison: water (– □ –); mud (– □□ –).

IMPACT/APPLICATIONS

The results of this combined field/laboratory/theory/modeling effort are field and lab data for model verification and testing and models for the propagation of water waves over regions of bottom mud. The dissipation due to a variety of mechanisms is included in the models; however, the most likely mechanisms will be determined from the field experiments. Laboratory experiments provide data to elucidate the mechanisms of energy transfer from the waves to the sediment

REFERENCES

Bentley, S.J., and Nittrouer, C.A., 2003, Emplacement, modification, and preservation of event strata on a flood-dominated continental shelf: Eel Shelf, northern California. *Continental Shelf Research*, 23: 1465-1493.

Dalrymple, R. A., and P. L. F. Liu (1978), Waves over soft muds: a two-layer fluid model, *Journal of Physical Oceanography, 8(6), 1121-1131*.

Elgar, S., and Raubenheimer, B., 2008, Wave dissipation by muddy seafloors, *Geophys. Res. Lett.*, 35, L07611, doi:10.1029/2008GL033245, 35(7), 1-5.

Huhe, A. and Huang, Z.H., 1994, An experimental study of fluid mud rheology—mud properties in Hangzhou Bay navigation channel. Part II. Beijing. Rep. No. 1. Institute of Mechanics, Chinese Academy of Sciences, 34-56. In Chinese.

Maa, P.-Y., 1986. Erosion of soft muds by waves. Report UFL/COEL-TR/059. Coastal & Oceanographic Engineering Department, University of Florida, Gainesville, 269pp.

Macquaker, J., Bentley, S.J., and Bohacs, K., 2010, Wave enhanced sediment-gravity flows and the dispersal of mud across continental shelves: a reappraisal of physical sedimentary processes operating in distal, “low energy” settings and their stratal record. *Geology* 38: 947-950.

Mei, C.C., Krotov, M, Huang, Z.H. and Huhe, A, 2010, Short and long waves over a muddy seabed, *Journal of Fluid Mechanics,* 643, 33-58.

Sheremet, A. & Stone, G., 2003, Observations of nearshore wave dissipation over muddy sea beds. *Journal of Geophysical Research* **108** (C11), 1-11.

Sheremet, A., Mehta, A., Liu, B. and Stone, G., 2005, Wave sediment interaction on a muddy inner shelf during Hurricane Claudette. *Estuarine, Coastal and Shelf Science* **63** (1-2), 225-233.

Traykovski, P. and Jaffre, F., 2011, Development and field measurements with multi-frequency, pulse-coherent Doppler systems, *The Journal of Ocean Technology*, Vol. 6, No. 2, 62-65.

Traykovski, P., P.L. Wiberg, and W.R. Geyer, 2007, Observations and modeling of wave-supported sediment gravity flows on the Po prodelta and comparison to prior observations from the Eel shelf. *Continental Shelf Research*, 27(3-4): 375-399.

Tsuruya, H. and Nakano, S. 1987, Interactive effects between surface waves and a muddy bottom. *Proceedings of the Conference on Advances in Understanding Coastal Sediment Processes*, ASCE: 50-62.

Yamamoto, T. and Schuckman, B. 1984, Experiments and theory of wave-soil interactions, *Journal of Engineering Mechanics*, ASCE, 110, 95-12.

PUBLICATIONS

Alam, M.-R., Liu, Y. and Yue, D. K. P., 2011, Attenuation of short surface waves by the sea floor via nonlinear sub-harmonic interaction. *Journal of Fluid Mechanics* [in press, refereed].

Hu, Y., Guo, X., Shen, L. and Dalrymple R.A., 2011, Direct numerical simulation of water wave propagating over viscous fluid mud, in review.

Hu, Y., Liu, Y., Shen, L. and Dalrymple R.A., 2011, Numerical study of breaking surface wave over muddy seabed, in preparation.

Macquaker, J., Bentley, S.J., and Bohacs, K., 2010, Wave enhanced sediment-gravity flows and the dispersal of mud across continental shelves: a reappraisal of physical sedimentary processes operating in distal, "low energy" settings and their stratal record. *Geology* 38: 947-950

Maxeiner, E. and Dalrymple, R.A., 2011, Experimental observations of standing interfacial waves induced by surface waves in muddy water, *Physics of Fluids* 23, 9: 96603; doi:10.1063/1.3639189

Yang, D. and Shen, L. 2011a, Simulation of viscous flows with undulatory boundaries. Part I: Basic solver, *Journal of Computational Physics*, **230**, 5488-5509.

Yang, D. and Shen, L. 2011b, Simulation of viscous flows with undulatory boundaries. Part II: Coupling with other solvers for two-fluid computations, *Journal of Computational Physics*, **230**, 5510-5531.